Hindawi
Journal of Chemistry
Volume 2018, Article ID 1764132, 10 pages
https://doi.org/10.1155/2018/1764132

Research Article

The Effect of Menisci on Kinetic Analysis of Evaporation for Molten Alkali Metal Salts ($CsNO_3$, CsCl, LiCl, and NaCl) in Small Cylindrical Containers

In-Hwan Yang, Hee-Chul Yang, and Hyung-Ju Kim

Decontamination & Decommissioning Research Division, Korea Atomic Energy Research Institute, Daejeon 34057, Republic of Korea

Correspondence should be addressed to In-Hwan Yang; ihyang@unm.edu

Received 2 November 2017; Revised 15 January 2018; Accepted 29 January 2018; Published 22 February 2018

Academic Editor: Jae Ryang Hahn

Copyright © 2018 In-Hwan Yang et al. This is an open access article distributed under the Creative Commons Attribution License, which permits unrestricted use, distribution, and reproduction in any medium, provided the original work is properly cited.

Using isothermal thermogravimetric data of alkali metal salts ($CsNO_3$, CsCl, LiCl, and NaCl), we conducted kinetic analysis on atmospheric evaporation to investigate the effect of meniscus on determining the condensation coefficient. In the process of evaporation into an atmospheric gas, molten salt decomposed at the interface between molten salt and an atmospheric gas reacts with chemical compositions of the atmospheric gas to be an equilibrium state. In this atmospheric evaporation, the interface shape of molten salts is affected by the container diameter and the contact angle at the container wall. In the analysis results, the formed concave/convex meniscus led to underestimating the condensation coefficient of molten salts. However, whether the values of the condensation coefficient of molten salts were affected by menisci, the range of the predicted values was still low from 10^{-3} to 10^{-5}. This result means that the presence of the foreign gas (air and Ar) is a dominant parameter in determining the condensation coefficient of atmospheric evaporation.

1. Introduction

There have been various researches on using molten salts as reaction and energy transfer medium for macro- and microscales of potential applications, because of the fascinating thermophysical and electrochemical properties of molten salts. Molten salts have relatively higher thermal stability and lower vapor pressure, compared to common solvents. These attractive properties have provided a wide and high operating temperature range, suppressing relevant mass loss with evaporation or decomposition at operating temperature. Examples include pyrochemical reprocessing of spent nuclear fuel [1, 2], molten salt electrolysis [3], heat transfer fluid in nuclear plant [4, 5], cooling medium for quenching process of alloys [6], alternative electrolytes in batteries [7], and thermal storage in solar thermal power plants [8, 9]. However, in spite of low vapor pressure of molten salts, there is inevitable loss with evaporation of metal species at higher operating temperature, which consequently affects the overall efficiency of the process.

To accurately predict this evaporation of molten salts, the kinetic theory of gas [10] has been widely used. In the kinetic theory of gas, the evaporation rate under the nonequilibrium condition is determined by the number of the gas molecules striking the surface from the equilibrium vapor and the actual gas pressure acting on the surface of the liquid phase. However, classic experimental studies [11–13] measuring the evaporation rate at the surface reported that the measured evaporation rate was lower than the value theoretically predicted by the kinetic theory of gas. To address this discrepancy between the theoretical predictions and experimental measurements with a correction coefficient, the Hertz-Knudsen equation [14–17] was suggested. As expressed in (1), the evaporation rate in the nonequilibrium condition is calculated by the pressure difference between the equilibrium vapor pressure, P^*, at temperature, T, and the pressure acting on the surface of the liquid phase, P, with the condensation coefficient, α.

$$\frac{dN}{dt} = \alpha \frac{(P^* - P)}{\sqrt{2\pi MRT}} A. \tag{1}$$

dN/dt is the evaporated molecular moles per unit of time, A is the cross-sectional area of the container, M

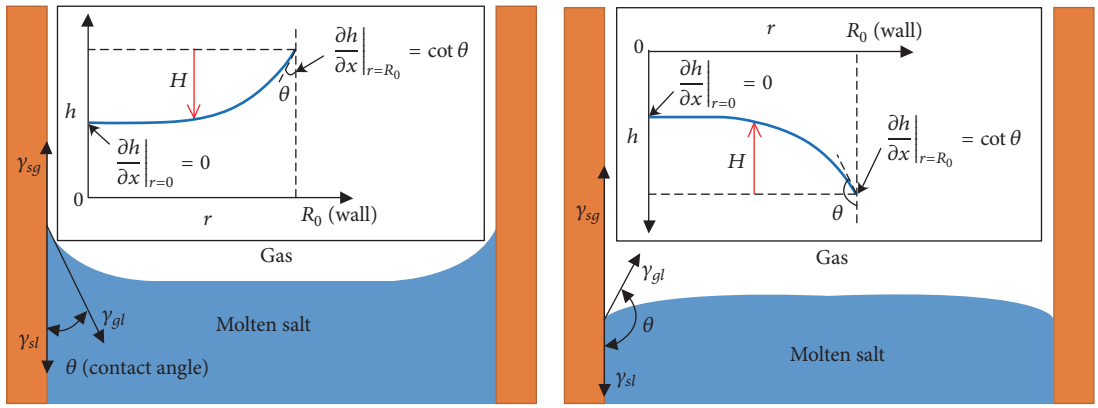

Figure 1: Schematic of the formed concave (a) and convex (b) meniscus of molten salts.

is molar mass, and R is the universal gas constant. The condensation coefficient used in the equation is effective for empirically correcting the predicted rate of evaporation into vacuum [16, 18, 19] or a gas atmosphere [1, 20–23]. However, determination of the coefficient values in numerous experimental studies on the evaporation process has produced inconsistency. In the case of water evaporation, for an example, the reported coefficient values varied from an order of 10^{-3} to 1 [24].

From the theoretical investigation on the inconsistency of the condensation coefficient [7, 25–30], it was suggested that the presence of a very thin layer above the surface of the condensed phase, known as the Knudsen layer, resulted from evaporation of the condensed phase. This very thin layer may work like diffusional resistance, reflecting gas molecules from the thin layer into the bulk gas phase. An equilibrium, therefore, cannot occur at the surface of the condensed phase but is achieved within the thin layer. This nonequilibrium within the Knudsen layer may cause the thermophysical properties of the layer, including density, pressure, and temperature, to diverge from those of the bulk gas phase, and consequently disturb determining the accurate condensation coefficient.

Based on this hypothesis that the condensation coefficient is the result of nonequilibrium within the Knudsen layer, several research groups have developed complicated models by modifying the Maxwell-Boltzmann distribution [25, 27] or by applying transition state theory [26]. These theoretical approaches for dealing with the effect of the Knudsen layer on the evaporation have managed to reduce the inconsistency of the condensation coefficient in the reported experimental results. However, the inconsistency of the condensation coefficient has not been fully resolved yet, because the analysis may leave behind unevaluated parameters, such as the meniscus.

This paper therefore examines experimental measurements of vaporization of alkali metal salts into an atmospheric gas in an attempt to quantify the effect of a meniscus on determining the evaporation flux and the condensation coefficient. The actual evaporation area associated with morphological changes of the meniscus in various diameters of cylindrical containers was predicted and characterized by using an analytical equation derived from the Young-Laplace law [31, 32]. The equilibrium vapor pressure at the surface used in the kinetic analysis of evaporation was also predicted by using the commercial thermodynamic equilibrium software, HSC chemistry 7.1 (Outotec) [33]. The predicted values of the condensation coefficient in various sizes of a cylindrical container were compared. Inconsistent values in the determined condensation coefficient revealed the effect of the meniscus on evaporation of the molten salts.

2. Materials and Methods

2.1. Evaporation Area of Molten Salts. The interface separating a molten salt and an atmospheric gas in a small container is not a flat interface but should be either concave or convex meniscus (Figure 1) due to the force balance along the interface. In the Young-Laplace law, the interfacial tension force, the normal force associated with the local curvature of the interface, is equated to the difference in the pressure exerted onto the interface by the molten salt and the atmospheric gas. The force balance is thus given as

$$\gamma \nabla \cdot n = \Delta P. \tag{2}$$

From the principle of the hydrostatic equilibrium, the term for the pressure jump across the interface in (2) can be replaced by the hydrostatic pressure of the molten salt and the atmospheric pressure. In the hydrostatic equilibrium state of the molten salt illustrated in Figures 1(a) and 1(b), the vertical gradient of the interface associated with the interfacial tension is equated to the hydrostatic pressure of the molten salt. Therefore, the curvature of the interface in (2) is rewritten as a function of the interface height from the horizontal reference plane where the hydrostatic pressure

equals the atmospheric pressure. The interface profile is finally expressed by the next equation.

$$\nabla \cdot n = \frac{d^2h/dr^2}{\left(1 + (dh/dr)^2\right)^{3/2}} = \frac{\rho g\left(h - h_{\text{ref}}\right)}{\gamma}. \quad (3)$$

Here γ is the surface tension between the molten salt and the atmospheric gas, ρ is the density of the molten salt, and h and h_{ref} are the height of the interface and the reference plane, respectively. Equation (3) can be linearized when the slope of the interface, dh/dr, is much less than unity [34]. The interface profile is thus simplified and then given as

$$\frac{d^2h}{dr^2} = \frac{\rho g\left(h - h_{\text{ref}}\right)}{\gamma}. \quad (4)$$

This equation is solved subject to boundary conditions: that is, the slope of the interface is zero at the center of the axisymmetric interface ($r = 0$), the interface forms a contact angle θ with the container wall ($r = R_0$), and the reference plane locates at the intersection between the interface and the container wall ($r = R_0$).

$$\left.\frac{dh}{dr}\right|_{r=0} = 0,$$
$$\left.\frac{dh}{dr}\right|_{r=R_0} = \cot(\theta), \quad (5)$$
$$h_{\text{ref}}|_{r=R_0} = 0.$$

In these conditions, the contact angle, θ, is the angle formed by the intersection between the interface of the solid-condensed phase and the interface of the gas-condensed phase at the container wall, as shown in Figure 1. This contact angle is an intrinsic property of the three-phase contact line between the molten salt, the atmospheric gas, and the container wall. Solving (3) in conjunction with the boundary conditions, the concave or convex meniscus can be expressed by the changes in the local elevation along the container radius. The local elevation of the interface, H, is expressed in terms of the radial position, r, contact angle, θ, as in the following equation:

$$H = \frac{2L_c}{e^{R_0/L_c} - e^{-R_0/L_c}} \cot(\theta) \cdot \left(\cosh\left(\frac{r}{L_c}\right) - \cosh\left(\frac{R_0}{L_c}\right)\right). \quad (6)$$

In the equation, the capillary length [35], L_c, is a characteristic length scale for an interface which is subject to the hydrostatic force ($\rho g L_c$) and the surface tension force (γ/L_c). When the capillary length is much larger than the diameter of the container, the surface tension force dominates the hydrostatic force at the interface of the molten salt. This capillary length is defined by the next equation,

$$L_c = \sqrt{\frac{\gamma}{\rho_l g}}. \quad (7)$$

The interface area is obtained by rotating its concave or convex meniscus, from the center of the axisymmetric interface to the cylindrical container wall, about the h-axis. The meniscus area, A_{meni}, becomes

$$A_{\text{meni}} = \int_0^{R_0} 2\pi r \sqrt{1 + \cot(\theta)^2 \operatorname{csch}\left(\frac{R_0}{L_c}\right)^2 \sinh\left(\frac{r}{L_c}\right)^2}\, dr. \quad (8)$$

In this study, the elliptic integral of (8) is solved numerically by using the commercial algebra software, Mathematica 9.0 (Wolfram Research Inc.) [36]. The calculated area is used as the actual evaporation area in the analysis for evaporation of the molten salts in small cylindrical containers.

2.2. Thermogravimetric Experiment. The vaporization rates of the molten cesium salts were measured by using a custom-made TGA (thermogravimetric analyzer). The TGA system used in this study mainly consists of a furnace equipped with a maximum weight capacity of 10 grams, a control and data acquisition system, and a gas feeding system. Gaseous atmospheres in the furnace are maintained by flowing compressed air at a rate of 1 L/min during conducting experiment. The exhaust gas from the furnace is scrubbed with multiple metal-vapor scrubbing impingers, as shown in Figure 2.

In the experiment for measuring the evaporation rate at constant temperatures, five grams of the sample salt loaded in a cylindrical crucible with an inner diameter of 21 mm was placed inside the TGA furnace and was heated with a constant rate of 20 K/min from room temperature to the investigated isothermal temperature. The dynamics of sample weight loss with time at an isothermal temperature was measured and recorded until the change of the sample mass became constant.

The experimental evaporation rates of CsCl and $CsNO_3$ were determined by

$$\frac{dN}{dt} = \frac{1}{M}\frac{dW}{dt}. \quad (9)$$

In the equation, M is the molecular mass of the sample cesium species and dW is the mass change during the differential time, dt. The evaporation rates were consistent during the experiment, except the start-up and shut-down process of TGA. Thus, the evaporation rates were determined by averaging their values over time, weight losses from 20% to 80% of the initial mass. The results of the isothermal TGAs for CsCl and $CsNO_3$ at five different isothermal temperatures and the parameters used in the experiment are summarized in Table 1.

In this paper, in addition to the conducted experimental measurement for evaporation rates of CsCl and $CsNO_3$, the reported data of alkali chloride species (NaCl and LiCl) [1, 22, 23] were also used to extend the present kinetic analysis of evaporation. Table 1 also includes the evaporation rates and the parameters used in the reported thermogravimetric experiments.

Table 1: Measured evaporation rates and experimental conditions used in isothermal thermogravimetric experiments for the molten alkali metal salts.

Molten salt	Temperature (°C)	Evaporation rate (mol/min)	Atmospheric Gas	Contact angle [37] (°)	Diameter of container (cm)
CsCl	850	1.39×10^{-5}	Air	31	2.1
	890	2.45×10^{-5}			
	930	4.28×10^{-5}			
	970	7.22×10^{-5}			
	1000	1.78×10^{-4}			
$CsNO_3$	500	3.29×10^{-5}	Air	22	2.1
	540	6.27×10^{-5}			
	580	1.12×10^{-4}			
	620	1.90×10^{-4}			
	660	3.08×10^{-4}			
LiCl [1, 22]	850	9.68×10^{-5}	Ar	136	3.0
	900	4.19×10^{-4}			
	950	4.19×10^{-5}			0.4
NaCl [23]	935	2.00×10^{-4}	Ar	113	3.81
	950	2.77×10^{-4}			
	985	4.03×10^{-4}			

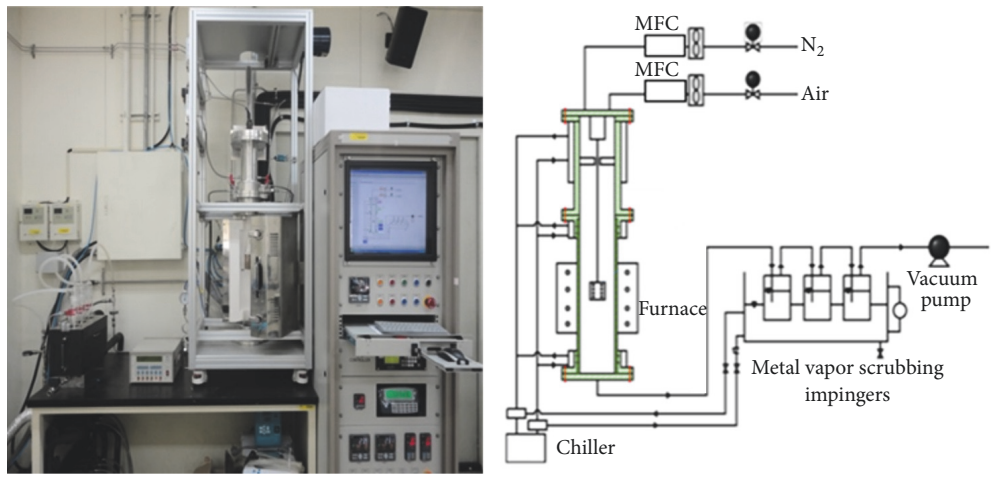

Figure 2: Image and schematic diagram of the TGA system used in this study.

3. Results and Discussion

3.1. Characterization of Meniscus. As indicated earlier, the profile of the interface between molten salt and atmospheric gas in a cylindrical container is directly determined by solving (6). The temperature dependent properties of the molten salts, such as the density and the interfacial tension coefficient, used the values found on the molten salts handbook [3]. The reported values from Baumli and Kaptay's measurement [37] were used for contact angles of the molten slats. The calculations for predicting the meniscus in an open cylindrical container with wide ranges of diameters (0.1 m–0.0005 m) were performed at the identical temperature conditions used in the thermogravimetric experiments. Figures 3(a) and 3(b) plot the local elevation of the interface, H, versus the dimensionless radial location, r/R_0, for NaCl at 950°C and CsCl at 1000°C, respectively.

The comparison of the interface profiles in these figures shows that decreasing the diameter of the container causes changes in the shape of the interface between the molten salt and the atmospheric gas. For all of the alkali metal salts used in the present calculations, as the diameter of the container decreases, the curvature of the interface, which is initially located near the container wall, starts to extend toward the center of the interface profile, reducing its flat portion. This change of the curvature finally leads the meniscus to be parabolic and then reduces the maximum elevation.

Based on the analysis results of the interface profile, the meniscus of the investigated molten salts can be classified into three basic regimes, namely, fully developed interface,

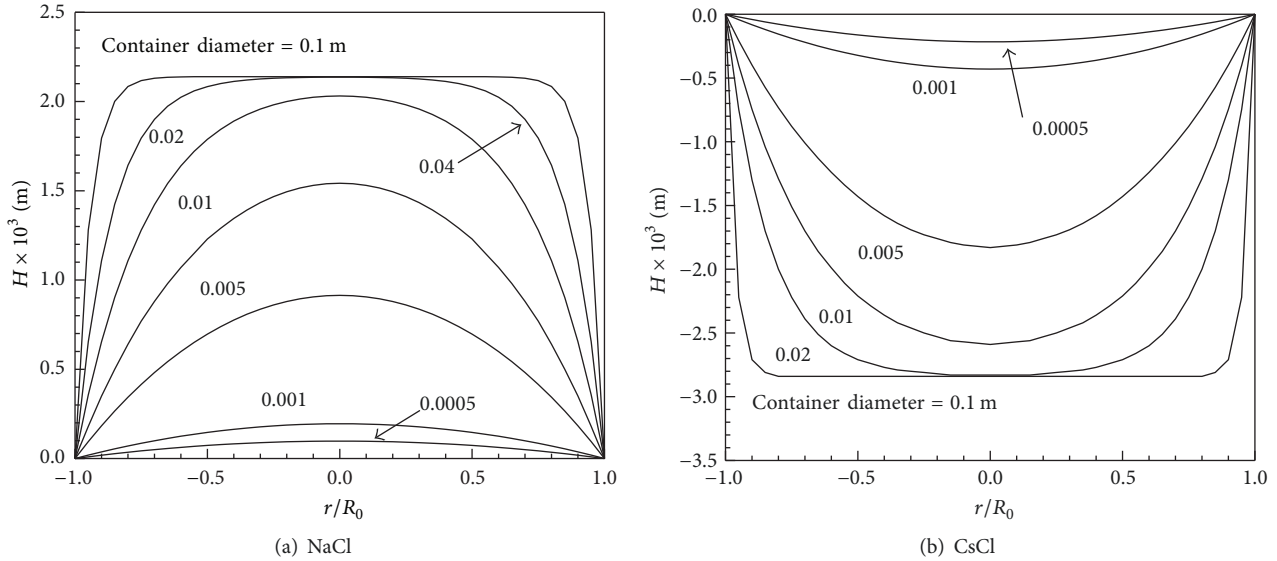

FIGURE 3: The meniscus profiles of molten NaCl at 950°C (a) and CsCl at 1000°C (b) in various diameters of cylindrical containers.

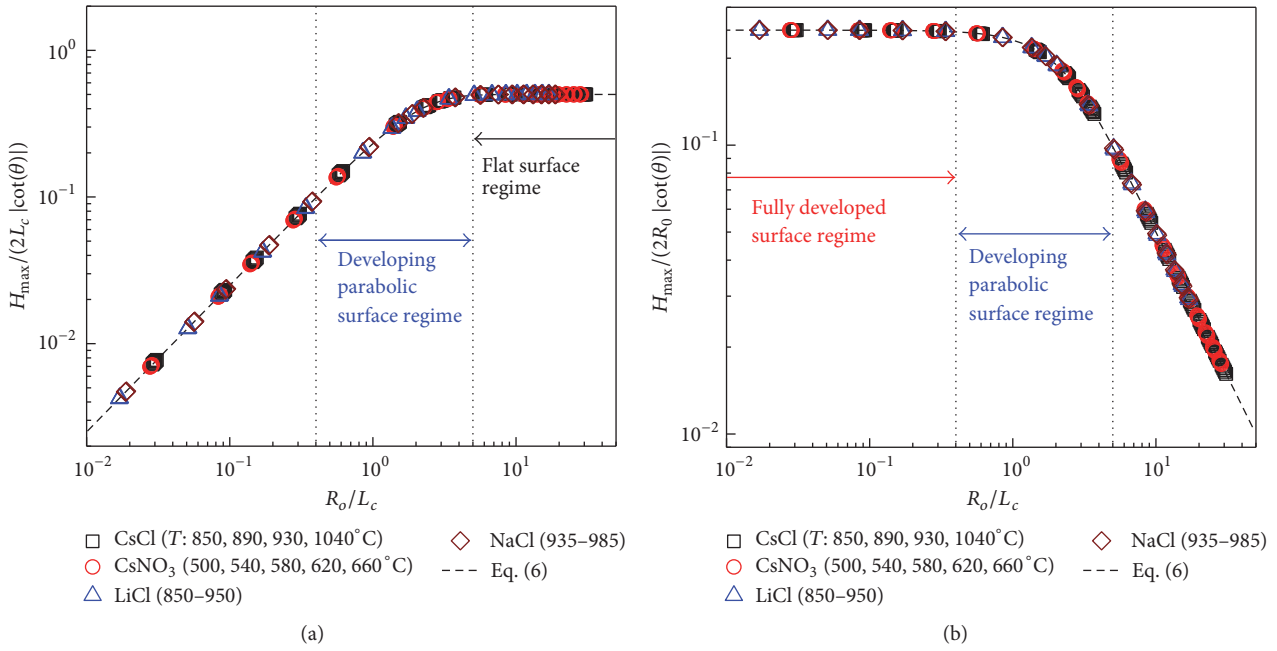

FIGURE 4: Maximum elevation ratio of molten salts to the capillary length (a) and to the container diameter (b) depending on the dimensionless radius of containers.

transition (or developing parabolic interface), and flat interface regime. Each interface regime is characterized by the dimensionless radius, which is the ratio of the container radius to the capillary length. In the flat interface regime, the gravitational force acting on the interface is dominant force over the interface. Thus, decreasing the container diameter decreases only the flat portion of the meniscus. In the maximum elevation, $H_{max}/(2L_c|\cot(\theta)|)$, presented in Figure 4(a), the values of each molten alkali metal salt are consistent when the ratio of the container radius to the capillary length is larger than 5.

Decreasing the values of the dimensionless radius (R_0/L_c) below 5 by decrease of the container diameter, the meniscus profile of the molten salts starts to evolve into a parabolic shape due to the extension of the interfacial tension force near the container wall. Figure 4(b) presents the results plotted in Figure 4(a) but plots the dimensionless elevation with respect to the container diameter; that is, $H_{max}/(2R_0|\cot(\theta)|)$. In the results, the boundary between the transition regime and the fully developed interface regime is identified by the changes in the gradient of the dimensionless elevation. The dimensionless elevation of the molten slats in the flat interface

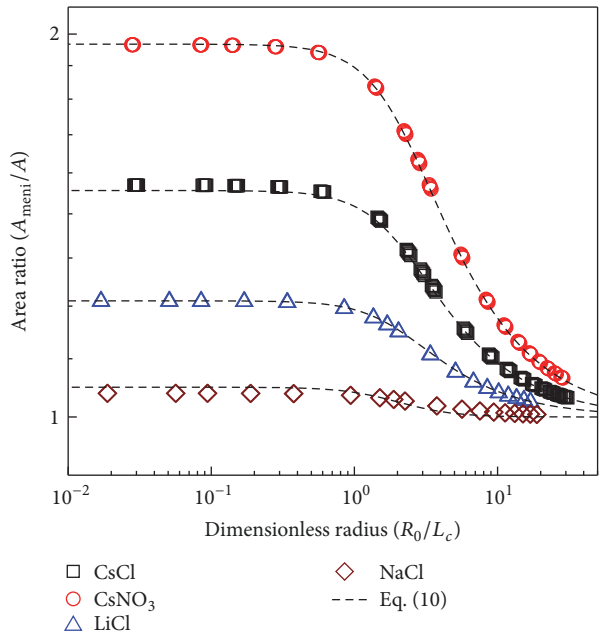

FIGURE 5: Comparison of semiempirical correlation (see (10)) with calculated values for the area ratio of the meniscus to the cross-section of container.

regime increases in exact proportion to the decrease of the container diameter, because the maximum elevation is not affected by the container dimension. However, after passing their flat interface regime, the gradients of the maximum elevation for all molten alkali metal salts start to decrease and then approach their asymptotic value of 0.25. Since the interface between the molten salt and atmospheric gas is completely governed by the interfacial tension force from the diameter corresponding to that value, further decrease in the radius of the container ($R_o/L_c < 0.4$) insignificantly affects the interface shape. It means that the changes of the maximum height are exactly proportional to that of the container radius in the fully developed interface regime.

3.2. Actual Evaporation Area in Containers. Figure 5 plots the area ratio of the meniscus to the horizontal cross-section of the container (A_{mani}/A) versus the dimensionless radius (R_0/L_c). Similar to the earlier results of the interface profile, the area ratio also decreases from its asymptotic value in the fully developed interface regime, as the dimensionless radius increases. For the meniscus in the flat interface regime, the curvature near the wall makes the interface area be also larger than the cross-sectional area of the container. However, this effect of the curvature decreases with more increase of the dimensionless radius, due to the increasing flat portion of the interface.

The comparison results in Figure 5 also show that the contact angle of the molten salt affects the values of the meniscus area where evaporation of molten salt occurs. The contact angle of molten salts, irrelevant in determining the interface shape regime, increases the value of the maximum elevation in proportion to the absolute value of $\cot(\theta)$. Using these compiled results of the analysis, a semiempirical correlation can be developed to account for the changes in the actual evaporation area of the molten salts in small cylindrical containers. The correlation is formulated in terms of the dimensionless radius of the container and the contact angle of molten salts at the container wall as

$$\frac{A_{meni}}{A} = 1 + \frac{0.222\,|\cot(\theta)|^{1.62}}{\left(1 + (0.5R/L_c)^{2.21}\right)^{0.445}}. \quad (10)$$

The empirical expression for the area ratio given by (10) is in excellent agreement with the predicted results.

3.3. Equilibrium Vapor Pressure and Maximum Evaporation Flux. Along with the experimental evaporation rate, the equilibrium vapor pressures of molten salts should be known to determine the condensation coefficient. In evaporation of molten alkali metal salts into a foreign gas, the condensed species could be decomposed at its surface and react with chemical compositions of an atmospheric gas in the evaporation process. If this chemical reaction occurs according to minimization of the total Gibbs free energy, that reaction represents an equilibrium state. The commercial thermodynamic calculations code, HSC chemistry 7.1, was therefore used for predicting the equilibrium composition of CsCl, $CsNO_3$, NaCl, and LiCl in an atmospheric gas (compressed air or argon gas). The air used in the calculations was composed of N_2 (78%), O_2 (20%), Ar (0.9%), and H_2O (1.1%). In the calculations, it was also assumed that the state of chemical equilibrium was maintained at the meniscus of molten salts with an atmospheric pressure. The thermodynamic calculation results of the equilibrium composition at the meniscus of each vaporizing species are summarized in Table 2.

The equilibrium compositions of the investigated alkali metal salts depending on the temperature are also plotted in Figure 6. In the predicted results of the equilibrium composition of the molten alkali metal salts, metal chloride species mainly evaporates into monomer (CsCl, LiCl, and NaCl), dimer (Cs_2Cl_2, Li_2Cl_2, and Na_2Cl_2), and trimer (Li_3Cl_3) and then become dominant species of the equilibrium gas phase. Other chemical species in each vaporization of molten salt also exists as an equilibrium species, but their concentrations are negligibly small in comparison with their dominant gas species as shown in the concentration distribution of equilibrium species (Figure 6).

In the calculated equilibrium composition of $CsNO_3$ (Figure 6(b)), however, the condensed phases of the cesium species such as $CsNO_3$, $CsNO_2$, and CsOH exist as equilibrium species together with each of their gaseous species as dominant species. These cesium species resulted from the reaction of $CsNO_3$ with chemical compositions of air, that is, expressed as the following reaction equations ((R1) and (R2)):

$$2CsNO_3 = 2CsNO_2 + O_2 \quad (R1)$$

$$4CsNO_3 + 2H_2O = 4CsOH + 2N_2 + 5O_2. \quad (R2)$$

The condensed phases of cesium species ($CsNO_3$, $CsNO_2$, and CsOH) are present in equilibrium with each of their

Table 2: Chemical species in the calculation of the equilibrium compositions of the molten alkali metal salts.

Vaporizing species	Condensed species	Gaseous species	Dominant gaseous species
CsCl	Cs, CsCl	Cs, Cs_2, CsCl, Cs_2Cl_2	CsCl, Cs_2Cl_2
$CsNO_3$	$CsNO_3$, $CsNO_2$, CsOH, CsO_2	$CsNO_3$, $CsNO_2$, CsOH, $Cs_2(OH)_2$, Cs, Cs_2O_2, CsO, Cs_2O, CsH, Cs_2	$CsNO_3$, $CsNO_2$, CsOH, $Cs_2(OH)_2$
NaCl	NaCl	NaCl, Na_2Cl_2, Na_3Cl_3, Na, Cl, Cl_2, Na_2, Cl_4, Cl_3	NaCl, Na_2Cl_2
LiCl	LiCl, Li_2Cl_2	LiCl, Li_2Cl_2, Li_3Cl_3, Li, Cl, Cl_2, Cl_4, Cl_3, Li_2	LiCl, Li_2Cl_2, Li_3Cl_3

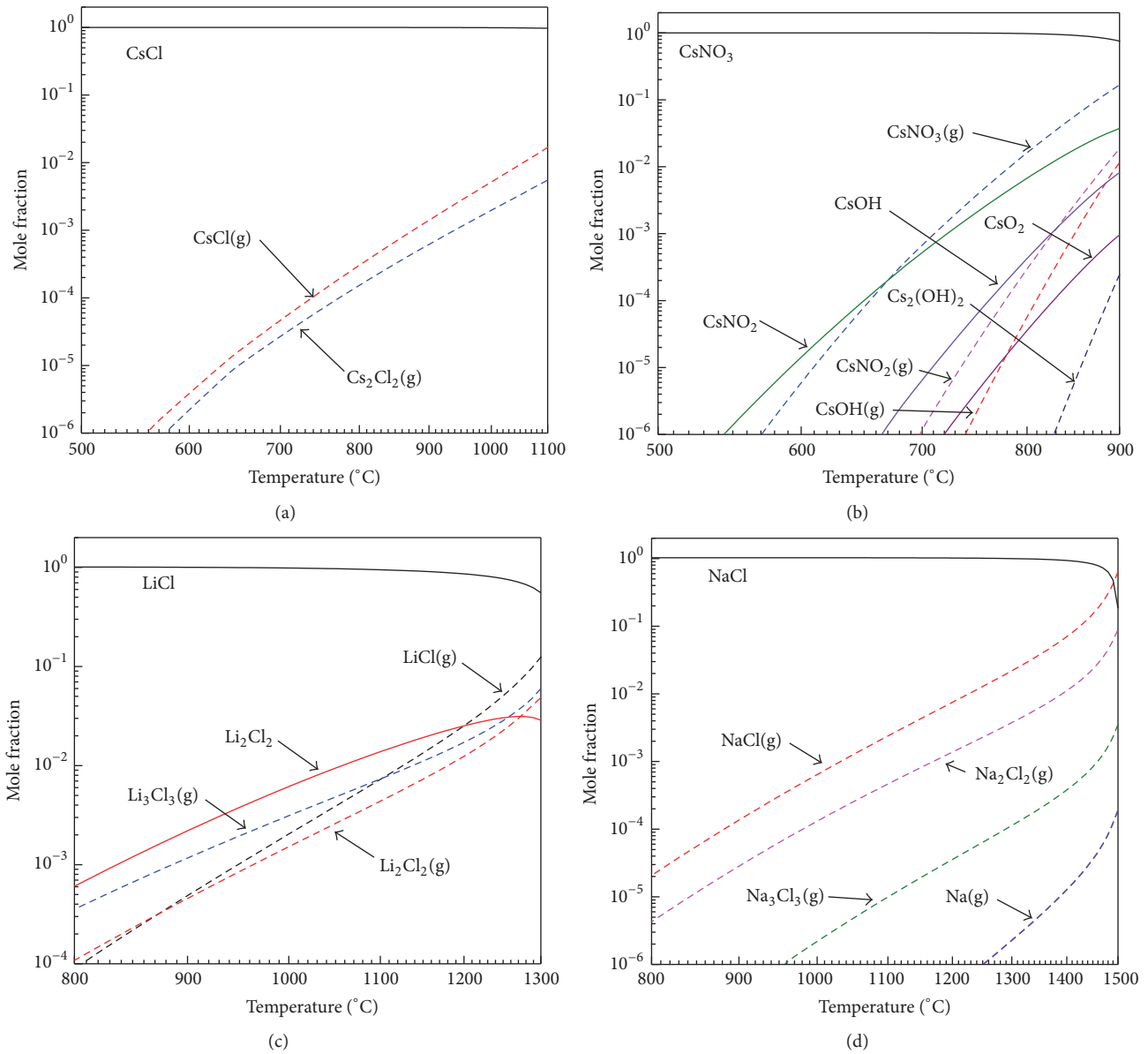

Figure 6: Calculated equilibrium compositions at the surfaces of molten CsCl (a), $CsNO_3$ (b), LiCl (c), and NaCl (d).

gaseous species at temperatures ranging from 550 to 900°C. $CsNO_3$ and $CsNO_2$ are in equilibrium with each of their gaseous species, and CsOH is in equilibrium with both the monomer and dimer forms of the gaseous cesium hydroxide in this temperature range.

From (1), the maximum mass flux from a molten salt to an atmospheric gas occurs when the condensation coefficient and the pressure acting on the surface of the liquid phase is unity and zero, respectively. The term for the vapor pressure of the condensed phase in (1) is equated to sum of

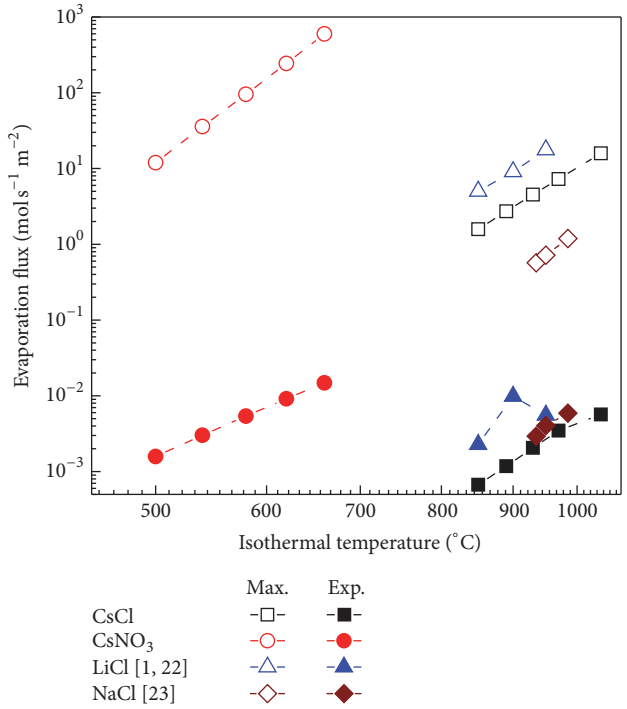

Figure 7: Comparison of the maximum theoretical vaporization fluxes and the experimental vaporization fluxes of the molten alkali metal salts (CsCl, $CsNO_3$, LiCl [1, 22], and NaCl [23]).

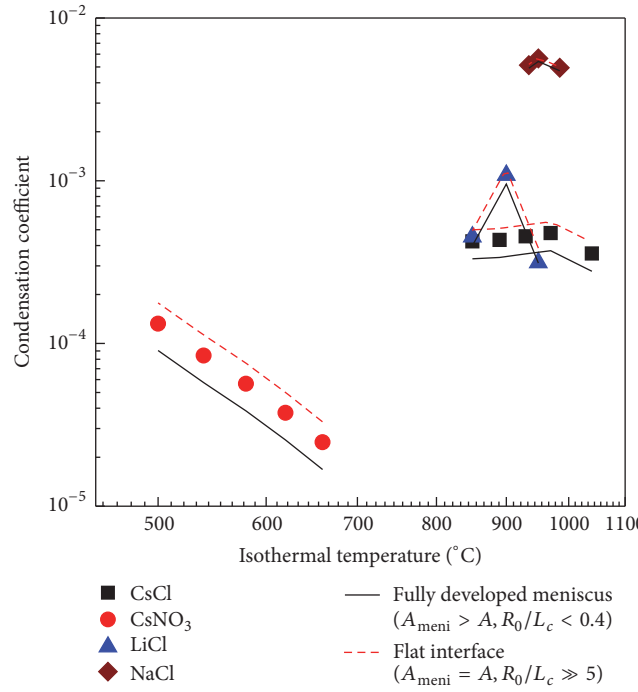

Figure 8: Comparison of the condensation coefficient of the molten alkali metal salts (CsCl, $CsNO_3$, LiCl, and NaCl).

equilibrium vapor pressure of monomer, dimer, and trimer species. Equation (1), therefore, can be expressed in terms of monomer species as

$$\frac{1}{A}\frac{dN}{dt} = \left(\frac{P_m^*}{\sqrt{2\pi M_m RT}} + \frac{2P_d^*}{\sqrt{2\pi M_d RT}} + \frac{3P_{tr}^*}{\sqrt{2\pi M_{tr} RT}}\right) \cdot \left(1 + \frac{0.222\,|\cot(\theta)|^{1.62}}{\left(1 + (0.5R/L_c)^{2.21}\right)^{0.445}}\right). \quad (11)$$

M is molar mass of monomer species, and subscripts m, d, and tr denote the monomer, dimer, and trimer species, respectively. The second term on the right hand side of (11) represents the area ratio of the molten salt surface to the cross-section of the container which accounts for the meniscus effect on the actual evaporation area.

The maximum theoretical vaporization flux of the molten salts obtained from (11) is compared with the experimental values determined from dividing the measured vaporization rate by the cross-sectional area of the container. In the thermogravimetric experiment, evaporation of the molten salts could be maximized by the purge gas flow which continuously removes vaporized gas species from the molten salt surface ($P = 0$). Therefore, the condensation coefficient of the molten salts can be determined by comparing the experimental flux to the maximum flux. Figure 7 shows the results of the molten salts comparing the values of the calculated maximum flux with the values obtained from the experiment and the reported data of Hur et al. [1], Kim et al. [22], and Baughman et al. [23]. The predicted values of the maximum theoretical flux are very large compared to those of the experimental flux.

3.4. Condensation Coefficient. Figure 8 presents the results of the condensation coefficient determined from the experimental flux data and the predicted maximum theoretical evaporation flux plotted in Figure 7. The values of the condensation coefficient at isothermal temperatures are the ratio of the maximum theoretical flux to the experimental flux. The experimental results show underestimation of the condensation coefficient for $CsNO_3$, CsCl, and LiCl. The maximum theoretical evaporation flux calculated from (11) underpredicts the values of the condensation coefficient, due to the meniscus effect on the evaporation area.

The results are also compared with the condensation coefficient curves predicted by using various sizes of containers. Decrease of the container radius makes the value of the condensation coefficient decrease at a constant temperature, due to the changes of the interface shape of the molten salts. However, this meniscus effect could not decrease the values of the condensation coefficient any more as the container radius is less than the critical radius for the fully developed interface ($R_0/L_c = 0.4$), such that the profile of the interface is fully developed (Figure 4).

The effect of the contact angle on determining the condensation coefficient of fully developed meniscus was presented by comparing the relative condensation coefficient of the molten slats. In the comparison results of Figure 9,

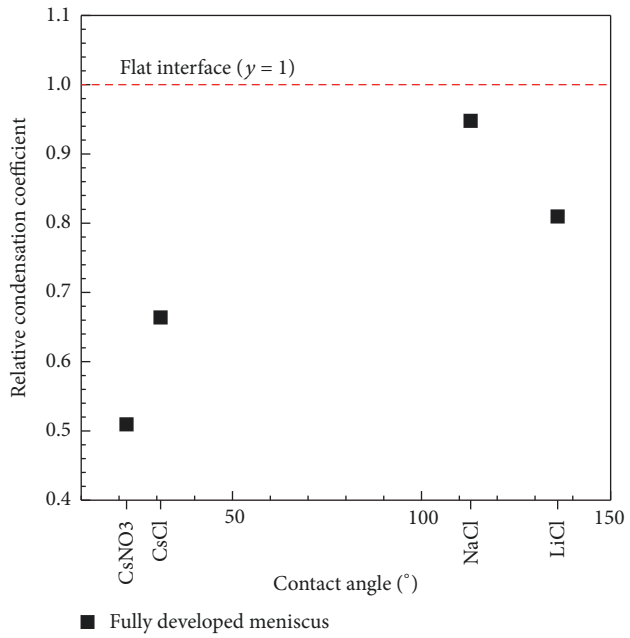

FIGURE 9: The relative condensation coefficient depending on the contact angle of fully developed meniscus of CsCl, $CsNO_3$, LiCl, and NaCl.

there is only 5% deviation in the condensation coefficient of NaCl relative to the value obtained from flat surface. However, for LiCl, CsCl, and $CsNO_3$, the deviation of the condensation coefficient increases by about 19%, 34%, and 49%, respectively, as the formed angle between the slope of the interface at the container wall and the horizontal plane increases.

The deviation of the condensation coefficient due to the morphological changes of the interface decreases as the container radius increases, or the contact angle is close to 90 degrees. This result suggests that assuming the cross-sectional area as an actual evaporation area would be invalid for the fully developed meniscus of the molten salt having higher or smaller contact angle at the container wall than 90 degrees. However, whether the condensation coefficient of all molten salts is affected by the interface shape, the range of their values is still from 10^{-3} to 10^{-5}. This result means that the presence of the foreign gas (air and Ar) would be a dominant parameter in determining the evaporation rate of alkali metal species. As the reported analysis on the mass transfer resistance of evaporation into atmosphere [20], the condensation coefficient of evaporation is the overall mass transfer resistance consisting of the atmospheric gas and the Knudsen layer, but the resistance values of the Knudsen layer are a hundred times lower than that of the atmospheric gas. It means that the contribution of the Knudsen layer to the values of the condensation coefficient is negligibly small even though the Knudsen layer is formed above the fully developed meniscus.

4. Summary and Conclusions

This paper has theoretically predicted the formed interface shape between the molten alkali metal salts and an atmospheric gas in the various diameters of small cylindrical containers and analyzed the meniscus effect on their evaporation. The deviation of the actual evaporation area from the cross-sectional area of small containers due to the meniscus decreases the predicted condensation coefficient. Results show that the meniscus of the molten salts is developing into a parabolic shape until the dimensionless radius is less than 0.4, increasing the area ratio of the meniscus with decreasing the container radius. However, after the meniscus is fully developed, decreasing the container radius negligibly affected the value of the area ratio of the meniscus to the cross-section of the container which was consistent but larger than unity.

The meniscus effect is important for accurately determining the condensation coefficient of molten salts. The values of the condensation coefficient of molten alkali metal salts were obtained from the experimental measurement and the reported analysis of the evaporation flux by Hur et al. [1], Kim et al. [22], and Baughman et al. [23], in conjunction with the analysis of the equilibrium vapor pressure. The meniscus effect on the evaporation of the molten salts could be quantified by comparing the condensation coefficients determined by using various diameters of cylindrical containers. The comparison results of the alkali metal slats show that the maximum decrement of the condensation coefficient due to the meniscus was $CsNO_3$ > CsCl > LiCl > NaCl, according to the angle formed at the intersection between the interface and the horizontal reference plane.

The meniscus effect of molten salts depending on the container radius and their contact angle at the container wall could significantly decrease the condensation coefficient by the changes in the actual evaporation area. However, considering the magnitude of the predicted condensation coefficient, it is suggested that the presence of a foreign gas would be a dominant resistance of mass transfer between a condensed phase and a gaseous phase in evaporation process of molten salts into a foreign gas.

Conflicts of Interest

The authors declare that they have no conflicts of interest.

Acknowledgments

This work was supported by the National Research Foundation of Korea (NRF) Grant funded by Korea government (MSIP) (no. NRF-2017M2A8A5015147).

References

[1] J.-M. Hur, S.-M. Jeong, and H. Lee, "Molten salt vaporization during electrolytic reduction," *Nuclear Engineering and Technology*, vol. 42, no. 1, pp. 73–78, 2010.

[2] Y. Sakamura, M. Kurata, and T. Inoue, "Electrochemical reduction of U O2 in molten Ca Cl2 or LiCl," *Journal of The Electrochemical Society*, vol. 153, no. 3, pp. D31–D39, 2006.

[3] G. J. Janz, *Molten Salts Handbook*, Academic Press, New York, NY, USA, 1967.

[4] C. W. Forsberg, P. F. Peterson, and P. S. Pickard, "Molten-salt-cooled advanced high-temperature reactor for production of

hydrogen and electricity," *Nuclear Technology*, vol. 144, no. 3, pp. 289–302, 2003.

[5] T. Abram and S. Ion, "Generation-IV nuclear power: a review of the state of the science," *Energy Policy*, vol. 36, no. 12, pp. 4323–4330, 2008.

[6] J. G. Speer, F. C. Rizzo Assunção, D. K. Matlock, and D. V. Edmonds, "The "quenching and partitioning" process: Background and recent progress," *Materials Research*, vol. 8, no. 4, pp. 417–423, 2005.

[7] H. Kim, D. A. Boysen, J. M. Newhouse et al., "Liquid metal batteries: Past, present, and future," *Chemical Reviews*, vol. 113, no. 3, pp. 2075–2099, 2013.

[8] U. Herrmann, B. Kelly, and H. Price, "Two-tank molten salt storage for parabolic trough solar power plants," *Energy*, vol. 29, no. 5-6, pp. 883–893, 2004.

[9] Z. Yang and S. V. Garimella, "Thermal analysis of solar thermal energy storage in a molten-salt thermocline," *Solar Energy*, vol. 84, no. 6, pp. 974–985, 2010.

[10] X.-T. Yan and Y. Xu, *Chemical Vapor Deposition: An integrated Engineering Design for Advanced Materials*, Springer, London, UK, 2010.

[11] E. H. Kennard, *Kinetic Theory of Gases with an Introduction to Statistical Mechanics*, McGraw-Hill, New York, NY, USA, 1938.

[12] M. Knudsen, "Die maximale Verdampfungsgeschwindigkeit des Quecksilbers," *Annalen der Physik*, vol. 352, no. 13, pp. 697–708, 1915.

[13] H. Hertz, "On the Evaporation of Liquids, Especially Mercury, in Vacuo," *Annals of Physics*, vol. 17, no. 177, 1882.

[14] A. H. Persad and C. A. Ward, "Expressions for the Evaporation and Condensation Coefficients in the Hertz-Knudsen Relation," *Chemical Reviews*, vol. 116, no. 14, pp. 7727–7767, 2016.

[15] P. Rahimi and C. A. Ward, "Kinetics of evaporation: Statistical rate theory approach," *Journal of Thermodynamics*, vol. 8, no. 1, pp. 1–14, 2005.

[16] C. T. Ewing and K. H. Stern, "Vaporization kinetics of solid and liquid silver, sodium chloride, potassium bromide, cesium iodide, and lithium fluoride," *The Journal of Physical Chemistry C*, vol. 79, no. 19, pp. 2007–2017, 1975.

[17] R. Hołyst, M. Litniewski, and D. Jakubczyk, "A molecular dynamics test of the Hertz-Knudsen equation for evaporating liquids," *Soft Matter*, vol. 11, no. 36, pp. 7201–7206, 2015.

[18] C. T. Ewing and K. H. Stern, "Equilibrium vaporization rates and vapor pressures of solid and liquid sodium chloride, potassium chloride, potassium bromide, cesium iodide, and lithium fluoride," *The Journal of Physical Chemistry C*, vol. 78, no. 20, pp. 1998–2005, 1974.

[19] J. Safarian and T. A. Engh, "Vacuum evaporation of pure metals," *Metallurgical and Materials Transactions A: Physical Metallurgy and Materials Science*, vol. 44, no. 2, pp. 747–753, 2013.

[20] H.-C. Yang, I.-H. Yang, M.-W. Lee, D.-Y. Chung, and J.-W. Choi, "Gas-surface interfacial and gas-phase resistances to vaporizing cesium hydroxide and chloride in air," *Vacuum*, vol. 123, pp. 86–90, 2016.

[21] K. Chatterjee, D. Dollimore, and K. S. Alexander, "Calculation of vapor pressure curves for hydroxy benzoic acid derivatives using thermogravimetry," *Thermochimica Acta*, vol. 392, no. 393, pp. 107–117, 2002.

[22] I. S. Kim, D. Y. Chung, M. S. Park, J. M. Hur, and J. K. Moon, "Evaporation of CsCl, BaCl2, and SrCl2 from the LiCl-Li2O molten salt of the electrolytic reduction process," *Journal of Radioanalytical and Nuclear Chemistry*, vol. 303, pp. 223–227, 2015.

[23] R. J. Baughman, R. A. Lefever, and W. R. Wilcox, "Evaporation of sodium chloride melts," *Journal of Crystal Growth*, vol. 8, no. 4, pp. 317–323, 1971.

[24] R. Marek and J. Straub, "Analysis of the evaporation coefficient and the condensation coefficient of water," *International Journal of Heat and Mass Transfer*, vol. 44, no. 1, pp. 39–53, 2001.

[25] T. Ishiyama, T. Yano, and S. Fujikawa, "Molecular dynamics study of kinetic boundary condition at an interface between argon vapor and its condensed phase," *Physics of Fluids*, vol. 16, no. 8, pp. 2899–2906, 2004.

[26] G. Nagayama and T. Tsuruta, "A general expression for the condensation coefficient based on transition state theory and molecular dynamics simulation," *The Journal of Chemical Physics*, vol. 118, no. 3, pp. 1392–1399, 2003.

[27] R. Meland and T. Ytrehus, "Evaporation and condensation Knudsen layers for nonunity condensation coefficient," *Physics of Fluids*, vol. 15, no. 5, pp. 1348–1350, 2003.

[28] A. V. Gusarov and I. Smurov, "Gas-dynamic boundary conditions of evaporation and condensation: numerical analysis of the Knudsen layer," *Physics of Fluids*, vol. 14, no. 12, pp. 4242–4255, 2002.

[29] G. Fang and C. A. Ward, "Temperature measured close to the interface of an evaporating liquid," *Physical Review E: Statistical, Nonlinear, and Soft Matter Physics*, vol. 59, no. 1, pp. 417–428, 1999.

[30] G. Fang and C. A. Ward, "Examination of the statistical rate theory expression for liquid evaporation rates," *Physical Review E: Statistical, Nonlinear, and Soft Matter Physics*, vol. 59, no. 1, pp. 441–453, 1999.

[31] E. Chibowski and R. Perea-Carpio, "Problems of contact angle and solid surface free energy determination," *Advances in Colloid and Interface Science*, vol. 98, no. 2, pp. 245–264, 2002.

[32] D. Y. Kwok and A. W. Neumann, "Contact angle interpretation in terms of solid surface tension," *Colloids and Surfaces A: Physicochemical and Engineering Aspects*, vol. 161, no. 1, pp. 31–48, 2000.

[33] *Proceedings of the International Symposium on Computer Software in Chemical and Extractive Metallurgy*, Elsevier, 1989.

[34] H. T. Davis, *Statistical Mechanics of Phases, Interfaces, and Thin Films*, VCH, New York, NY, USA, 1995.

[35] P.-G. Gennes, F. Brochard-Wyart, and D. Quere, *Capillarity and Wetting Phenomena: Drops, Bubbles, Pearls, Waves*, Springer, New York, NY, USA, 2002.

[36] Wolfram research Inc. Wolfram Mathmatica 9.0. 2013.

[37] P. Baumli and G. Kaptay, "Wettability of carbon surfaces by pure molten alkali chlorides and their penetration into a porous graphite substrate," *Materials Science and Engineering: A Structural Materials: Properties, Microstructure and Processing*, vol. 495, no. 1-2, pp. 192–196, 2008.

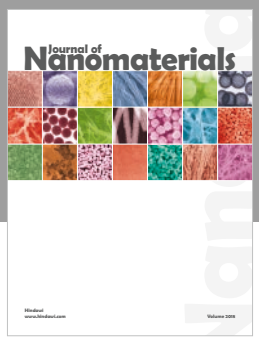

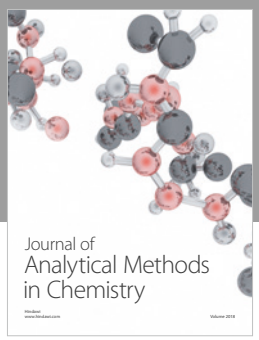

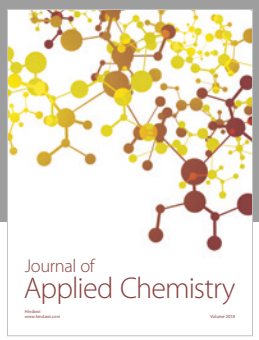

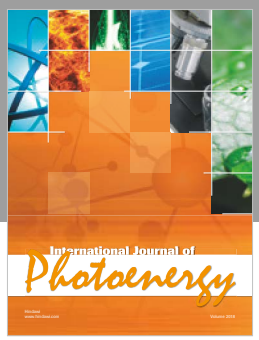

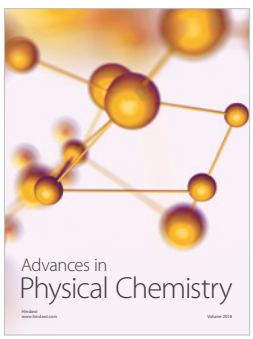

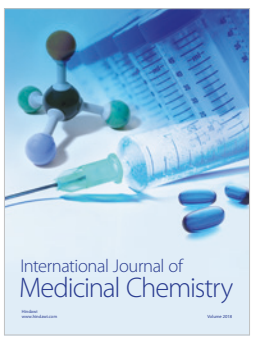

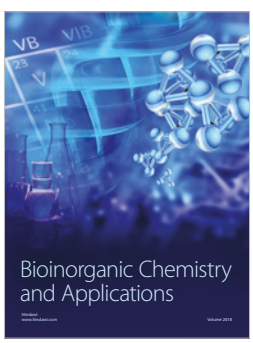

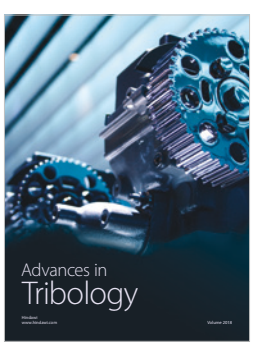

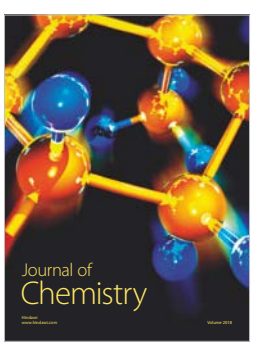

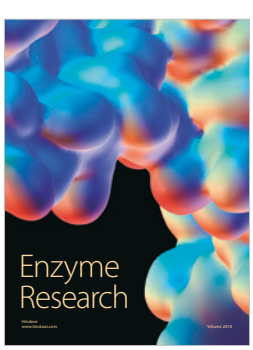

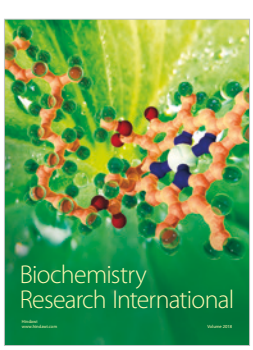

Hindawi

Submit your manuscripts at
www.hindawi.com